Taylor & Francis
Taylor & Francis Group

Nuclear Science and Engineering

ISSN: (Print) (Online) Journal homepage: www.tandfonline.com/journals/unse20

Radiation Protection and Shielding Analysis of the Versatile Test Reactor

Tingzhou Fei, Zhaopeng Zhong, Samuel E. Bays & Florent Heidet

To cite this article: Tingzhou Fei, Zhaopeng Zhong, Samuel E. Bays & Florent Heidet (2022) Radiation Protection and Shielding Analysis of the Versatile Test Reactor, Nuclear Science and Engineering, 196:sup1, 98-109, DOI: 10.1080/00295639.2021.1991760

To link to this article: https://doi.org/10.1080/00295639.2021.1991760

Published online: 01 Dec 2021.

NUCLEAR SCIENCE AND ENGINEERING · VOLUME 196 · S98–S109 · SUPPLEMENT 1 · 2022

DOI: https://doi.org/10.1080/00295639.2021.1991760

Radiation Protection and Shielding Analysis of the Versatile Test Reactor

Tingzhou Fei,[a]* Zhaopeng Zhong,[a] Samuel E. Bays,[b] and Florent Heidet[a]

[a]*Argonne National Laboratory, Lemont, Illinois*
[b]*Idaho National Laboratory, Idaho Falls, Idaho*

Received August 16, 2021
Accepted for Publication October 7, 2021

Abstract — *The Versatile Test Reactor (VTR) is currently under development by the U.S. Department of Energy. It will provide very high fast neutron flux irradiation capabilities that are currently unavailable in the United States. Given the increasingly large number of advanced reactor concepts being pursued in recent years, this irradiation testing capability will be essential to support maturation of these designs. Radiation protection is an important part of the VTR design. High neutron fluxes can pose a challenge for radiation protection of the structures and equipment near the reactor core. This paper provides a summary on the status of the radiation protection considerations and shielding analysis performed for VTR under a nominal operating condition. The main radiation sources identified and examined in the study are applicable only under this operating condition. The paper focuses on three areas of radiation protection and shielding: secondary sodium activation in the intermediate heat exchanger, air activation in the reactor vessel auxiliary cooling system, and dose rate above the head access area due to primary sodium activation. VTR design and development are continuously progressing, and as such, the shielding considerations discussed in this paper will evolve alongside the overall VTR design.*

Keywords — *Shielding analysis, Versatile Test Reactor, sodium activation.*

Note — *Some figures may be in color only in the electronic version.*

I. INTRODUCTION

The Versatile Test Reactor (VTR) is currently under development by the U.S. Department of Energy (DOE). It will provide very high fast neutron flux irradiation capabilities that are not readily available in the United States. The goal to achieve high neutron flux also poses a challenge for radiation protection of the structures and equipment near the reactor core. Thus, shielding analysis is an important part of the VTR design work. In this study, dose rate and activities were assessed at the different locations of interest based on the conceptual VTR design. The performance characteristics of the shields used to protect workers and reactor components from damaging radiation sources were evaluated in this work. The major radiation source in VTR during operation comes from the neutrons and photons emitted from nuclear fuel fissions as well as the activated primary coolant.

One shielding challenge for a pool-type Sodium-cooled Fast Reactor (SFR) such as VTR is activation of the secondary sodium. Intermediate heat exchangers (IHXs) are placed in the primary sodium pool inside the reactor vessel, and neutrons produced in the core can reach the IHXs due to the small absorption cross section of sodium and the large mean free path of fast neutrons.

*E-mail: tfei@anl.gov

The secondary sodium gets activated inside the IHX and carries through the entire secondary coolant system, which is in parts outside of the reactor vessel. This source of radioactivity needs to be limited or shielded against in order to meet the radiation dose limit set for personnel working at the plant.

Air activation in the reactor vessel auxiliary cooling system (RVACS) was also analyzed. The air flowing in the system gets close to the reactor core, and some elements such as argon will become activated and released into the atmosphere.

Last, even though workers will have only limited access to the head access area (HAA) directly above the reactor vessel, design efforts need to ensure that the dose rate received from the activated primary sodium will be below the set dose limits.

II. REACTOR AND SHIELDING

The reference conceptual VTR core design, detailed in Ref. 1, contains 114 reflector assemblies as well as 114 shield assemblies, arranged as shown in Fig. 1. The radial reflectors are arranged in three rows and contain 80.0% HT9 and 20.0% Na by volume. The radial shields are arranged in two rows and contain 36.3% B_4C, 28.3% HT9, and 24.3% Na by volume. As a key assumption for this set of analyses, the B_4C in the shield assembly uses natural boron. The reference VTR core generated 300 MW(thermal), and the corresponding flux level and distribution are used as the starting point for the shielding analyses.

The radial reflector and shield assemblies serve the purpose of reducing the radiation damage on the barrel wall by reducing the neutron leakage in the radial direction. They also help reduce the secondary sodium activation rate in the IHX and the air activation rate in the RVACS. Each fuel assembly, postulated test assembly, and control rod assembly contains a 90-cm lower reflector that is placed below the level where the active fuel region ends. The main purpose of the lower reflectors is to reduce the radiation damage on the upper grid plate.[2] Fuel assemblies and postulated test assemblies contain a 60-cm upper reflector placed above the gas plenum. This aims at reducing the neutron leakage from the top of the core and therefore help reduce component damage and the secondary sodium activation rate in the IHX. The relative positions of the axial reflectors in the test assemblies and control rods are discussed in more detail in Ref. 1.

The reactor design is based on the PRISM design.[3] In-vessel fixed shield structures are also present to further mitigate the secondary sodium activation in the IHX and the air activation in the RVACS. The in-vessel shield MCNP model is presented in Fig. 2. All the pieces of the shield arrangement work together to reduce the secondary sodium activation in the IHX. At the same time, they contribute to reducing the air activation in the RVACS. The shields placed around the core inlet plenum are mainly needed for limiting air activation in the

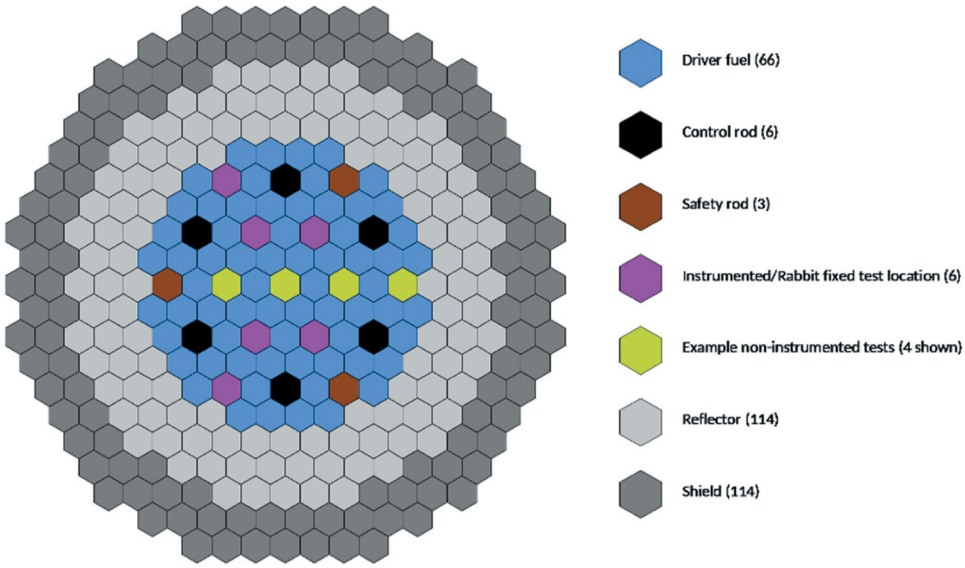

Fig. 1. VTR core radial layout.

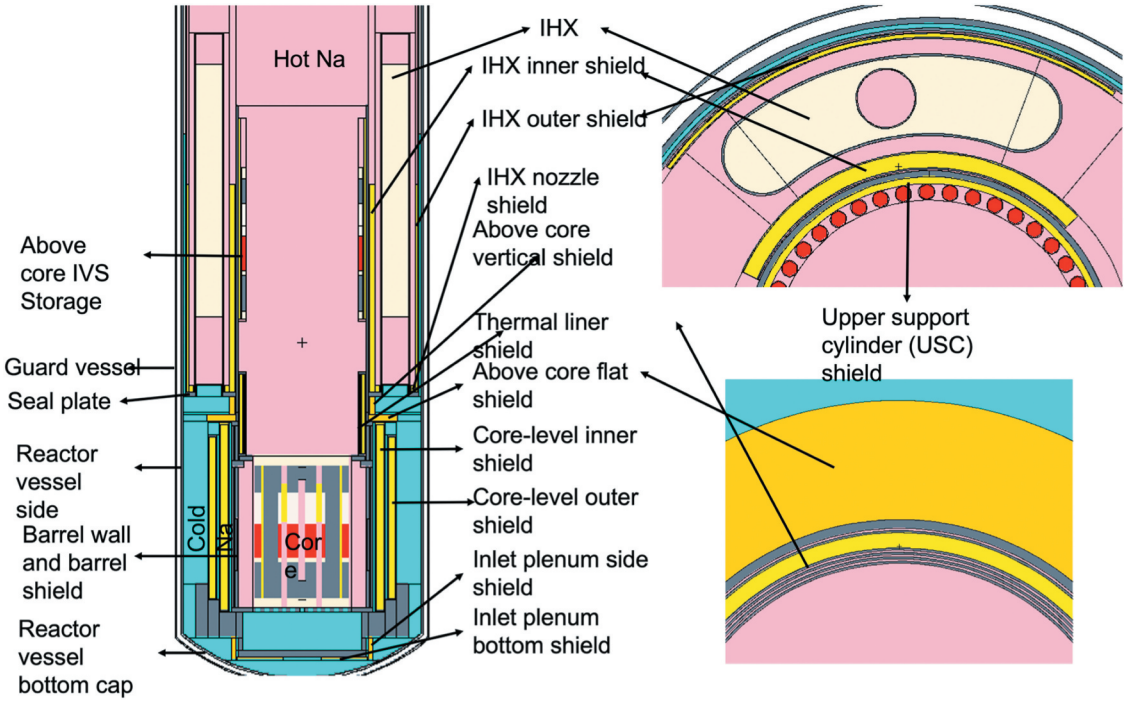

Fig. 2. In-vessel shield configuration for VTR.

RVACS and the radiation damage on the reactor vessel bottom.

The peak displacements per atom (dpa) and fast fluence on the reactor vessel were evaluated using the MCNP6.2 code[4] and the ADVANTG code.[5] The peak dpa and the fast fluence on the bottom hemispherical cap (shown in Fig. 2) of the reactor vessel are 2.12E-04 and 1.52E+17 n/cm^2 for 60 years of operation at 90% capacity factor (i.e., 54 effective full-power years). The peak occurs at the tip of the hemispherical cap. The peak DPA and the fast fluence on the side of the reactor vessel are 6.85E-05 and 1.21E+17 n/cm^2, respectively. Because of the extensive use of radial shields, the peak neutron flux on the reactor vessel occurs at the bottom hemisphere of the reactor vessel. The assembly receptacles in the inlet plenum are not included in the current model for conservatism. The effect of including the receptacles is expected to be small as the volume fraction of the receptacles in the inlet plenum region is expected to be less than 10%.

It is intended that as used fuel assemblies are discharged from the active core region, they would be stored in the radial shield region of the core as well as in the in-vessel storage (IVS) above the core as illustrated in Fig. 2. For this study, it was conservatively assumed that the total number of discharged assemblies that might be stored inside the vessel could be as high as 100. More details on that topic are discussed in Ref. 6. Here, we assumed that about 50 used fuel assemblies would be stored in the IVS and the rest in the radial shield region. In the MCNP6.2 model, the composition of these assemblies is assumed to be the core-average fuel composition at the beginning of the equilibrium cycle.

III. METHODOLOGY

The shielding analyses performed in this study follow a three-step process. In the first step, the radiation source characteristics such as the radiation particle types, and the source spatial, spectral, and angular distribution are evaluated. The second step identifies the location of interest for estimating dose rate, activation rate, or structural damage evaluation. In the last step, the actual particle transport calculation is performed for various shielding designs and sensitivity studies on the shield dimensions (thickness, height, etc.). This last step usually involves using variance reduction techniques to reduce the statistical uncertainties associated with the quantities of interest.

The MCNP6.2 Monte Carlo code was employed to perform neutron and photon transport calculations,

leveraging its ability to use a continuous energy neutron cross section and to model flexible geometry. For the fission neutron source during reactor normal operation, the eigenvalue mode was first called in MCNP6.2 to generate the volumetric fission neutron source. The subsequent shielding analyses were transformed to solve fixed source problems by using the created volumetric fission neutron source and turning off the neutron production from fission in the active core region. This source is the main contributor to the secondary sodium activation and the air activation. Above the HAA, the main contribution to the dose rate is from the primary sodium activation. In this case, the primary sodium activation rate was first evaluated using the core neutron source, and then, the photon transport calculation was performed using the activated primary sodium source.

For Monte Carlo codes, the shielding analyses are deep penetration problems. The regions of interest for these problems are usually heavily shielded and far away from the source. Therefore, only an extremely small fraction of the simulated source particles reaches the "detecting" region in an analog Monte Carlo simulation. Variance reduction techniques, such as the weight window technique,[7] are required for the Monte Carlo calculations to obtain tallies with sufficiently low statistical uncertainties with reasonable computation time. The weight windows needed for the MCNP6.2 calculation were generated with the ADVANTG code. This code uses a deterministic method to solve the multigroup adjoint neutron flux for a simplified VTR model, which allows building the importance map (weight window) that is then used by the MCNP6.2 code.

The sodium and air activations are evaluated using the flux tallies in MCNP6.2. The dose rate was calculated by converting the flux using the built-in flux-to-dose conversion factors in MCNP6.2 (Ref. 8).

IV. SECONDARY SODIUM ACTIVATION

The objective of the study is to estimate the secondary sodium activity in the secondary loop. The secondary sodium flowing in the IHX is activated through capture and $(n,2n)$ reaction by neutrons streaming from the reactor core. After capturing a neutron, ^{23}Na becomes ^{24}Na, which decays with a half-life of 14.96 h and emits two photons of energy 1.368 MeV/decay and 2.754 MeV/decay, respectively. Created from the ^{23}Na $(n,2n)$ reaction, ^{22}Na decays with a half-life of 2.60 years and emits a photon with an energy of 1.274 MeV. The ^{22}Na activity is much smaller than the ^{24}Na activity during normal operation due to the smaller cross section of the $(n,2n)$ reaction that leads to a smaller equilibrium ^{22}Na concentration. As the activated secondary sodium flows outside of the reactor vessel, its maximum activity level is constrained by the dose rate limits of areas around the secondary loop.

IV.A. Derivation of Sodium Activity Limit

The relation between the dose rate limit and the sodium activity limit depends on the secondary sodium pipe thickness, the potential shield thickness around the pipe, the pipe radius, and the distance from the pipe where the dose rate limit is imposed. The relation between the two limits was determined with the MCNP6.2 code. The photon released from the activated secondary sodium is assumed to be distributed uniformly inside the pipe. The dose rate at different distances away from the outer pipe surface was evaluated with the MCNP6.2 code assuming the pipe is infinitely long.

Annual occupational dose limits for workers at 5 rems of total effective dose have been established in 10 CFR 835.202.[a] This dose is administratively restricted by site procedure to 0.7 rem of total effective dose. This is about 0.34 mrem/h assuming 40 working hours/week, which corresponds to the value used by several other facilities. Based on this assumption, the secondary sodium activity limits are listed in Table I. The activity limits were derived from the dose rate limit at different distances from the secondary pipe. This limit is imposed on the secondary sodium at the exit from the reactor vessel for conservatism since the activity of the activated sodium will decay in the secondary loop outside the reactor vessel. A safety margin needs to be applied to

TABLE I

Secondary Sodium Activity Limits for VTR

Distance from the Pipe Outer Surface	^{24}Na Activity Limit (μCi/cm^3)
At the surface	2.88E-04
1 m from the surface	1.36E-03
2 m from the surface	2.54E-03

[a] *Code of Federal Regulations*, Title 10, "Energy," Part 835, "Occupational Radiation Protection," Sec. 202, "Occupational Dose Limits for General Employees," U.S. Nuclear Regulatory Commission.

account for the uncertainties associated with the model and the methods. A factor of 1.5 to 3 is suggested based on the shielding benchmark analyzed in the past[9] and as part of the ongoing verification and validation work for VTR.

IV.B. Method to Calculate Equilibrium Sodium Activity

During reactor operation, the secondary sodium activity reaches equilibrium when the activation rate is equal to the decay rate. It takes several hours to reach the equilibrium. The secondary sodium activity was evaluated approximately by solving the one-dimensional (1-D) particle transport Eq. (1):

$$\frac{DN(t,z)}{Dt} = \frac{\partial N(t,z)}{\partial t} + v\frac{\partial N(t,z)}{\partial z} = S - \lambda N \ , \qquad (1)$$

where

N = total population of the radionuclide of interest (^{24}Na/^{22}Na in this case)

v = 1-D coolant flow velocity

λ = decay constant of the radionuclide

S = production rate of the radionuclide, which was calculated by MCNP6.2.

At equilibrium, the Eulerian time derivative is zero, so Eq. (1) becomes

$$v\frac{\partial N(t,z)}{\partial z} = S - \lambda N \ . \qquad (2)$$

The problem consists of two regions. Region 1 lies inside the reactor vessel with a constant production term. Region 2 is outside the vessel, and the source is zero. Thus, for Region 2, the source term S is 0. Applying the boundary condition (at Region 1 start or Region 2 end, $N = N_2$, and at Region 1 end or Region 2 start, $N = N_1$), the equilibrium activity can be obtained by solving the solution of the ordinary differential equation:

$$N_1 = \left(N_2 - \frac{S}{\lambda}\right)e^{-\lambda t_1} + \frac{S}{\lambda} \ ,$$

where

$$N_2 = N_1 e^{-\lambda t_2} \ .$$

Then, at the exit of Region 1 (where the secondary sodium exits the reactor vessel), the ordinary differential equation can be expressed as

$$\lambda N_1 = \frac{S\left(1 - e^{-\lambda t_1}\right)}{1 - e^{-\lambda(t_1+t_2)}} \ , \qquad (3)$$

where t_1 and t_2 are the time spent by the secondary sodium inside and outside the reactor and λN_1 is the activity of the activated secondary sodium.

IV.C. Sodium Activity Calculation

Based on the methods described above, the secondary sodium equilibrium activity was evaluated for different configurations. The parameters that have a major impact on the secondary sodium activity include the IHX elevation relative to the active fuel, the distance between the upper support cylinder (USC) shield and thermal liner shield, the thickness of the core-level shield, and the USC and thermal liner shield elevation. The effects of the changes were investigated by incorporating individual changes sequentially. The results are listed in Table II.

The reasons driving these large activity changes can be explained better with the support of Fig. 3. There are two major neutron streaming paths reaching the IHX. Neutrons can escape the core from the top and penetrate through the USC shields, the used fuel, and the IHX inner shields to reach the IHX. The used fuel has very little effect on attenuating the neutrons. Lowering the USC and thermal liner shield elevation, increasing the gap between the USC and thermal liner shield, and reducing the IHX elevation would all increase the number of neutrons reaching the IHX through this path.

The other major streaming path for neutrons to reach the IHX is through the core-level shields. The neutrons escape the core in the radial direction, penetrate through the core-level shields, and move upward to reach the bottom of the IHX. Thus, reducing the thickness of the core-level shields or the IHX elevation would increase the number of neutrons reaching the IHX through this path.

IV.D. Effect of Heterogeneous Shield

In Sec. IV.C., the shields in the model are all modeled with homogenized compositions. This section examines the effect of modeling the shields explicitly with a heterogeneous model rather than with the homogeneous approach used to this point. The homogeneous models

TABLE II

Secondary Sodium Activity Evaluated for Different Configurations

Case Number	Description	Activity (μCi/cm^3)	Relative Error
0	Based on the most recent VTR design, includes major components (shields, structural walls, components, etc.).	2.38E-4	2.9%
1	Exclude the UIS in the model.	3.53E-4	3.4%
2	Based on Case 0, reduce the IHX elevation by 60 cm.	8.26E-4	1.4%
3	Based on Case 1, reduce the gap size between the USC and thermal liner shield by 35 cm.	2.61E-4	8.3%
4	Based on Case 3, increase the core-level shield thickness by 5 cm each for both inner and outer shields.	1.32E-4	4.3%
5	Based on Case 4, raise the elevation of the USC and thermal liner shield by 60 cm.	3.05E-4	3.3%

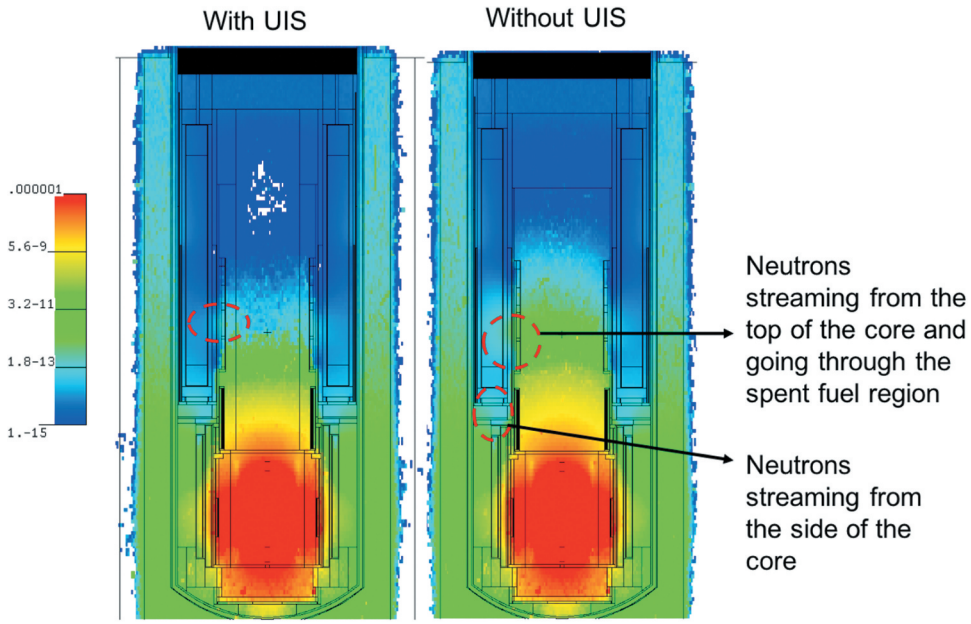

Fig. 3. Neutron flux comparison for (a) Case 0 with UIS and (b) Case 1 without UIS. The neutron streaming from the top of the core is circled for comparison. There is no change in the neutrons streaming from the side of the core.

filled the shield region with a homogenized mixture, which consists of steel, B_4C, and sodium with different volume fractions calculated from the actual dimensions. Each shield region is filled with different shield mixtures (different volume fractions of materials). In the heterogeneous model, the poison rod, the steel cladding, and the shield shells are all explicitly modeled. This assessment was performed for the IHX and the core-level inner and outer shields, and results are listed in Table III.

Overall, it is observed that the impact of modeling the shields heterogeneously is small, especially for the IHX outer shield. The numerical difference between the heterogeneous and homogeneous IHX outer shields is within the statistical uncertainty of the MCNP calculations. The heterogeneity effect of the IHX inner shield is larger and leads to an increase of the secondary sodium activation rate by about 12%. This is slightly larger than 3σ, meaning that the increase observed is statistically meaningful. The difference is due to the streaming effect of neutrons in the heterogeneous IHX inner shield model. There are only three rings in the IHX inner shield as shown in Fig. 4. However, to determine the actual increase would require us to obtain MCNP tallies with much lower statistical uncertainty (<1%). This requires intensive computational resources to reduce the statistical uncertainty to 1%, and the 10% to 20% difference

TABLE III

Secondary Sodium Activity for Heterogeneous and Homogeneous Shield Models

IHX Shield		Core-Level Shield			
Inner	Outer	Inner	Outer	Activity ($\mu Ci/cm^3$)	Relative Error
Hom.[a]	Hom.	Hom.	Hom.	2.38E-04	2.86%
Het.	Hom.	Hom.	Hom.	2.66E-04	2.54%
Het.	Het.	Hom.	Hom.	2.69E-04	4.00%
Het.	Het.	Het.	Het.	2.12E-04	2.73%
Hom.	Het.	Hom.	Hom.	2.42E-04	2.28%
Hom.	Hom.	Het.	Hom.	2.22E-04	2.49%
Hom.	Hom.	Hom.	Het.	2.06E-04	2.15%
Hom.	Hom.	Hom.	Het.[b]	1.99E-04	1.94%

[a]Hom. = homogeneous shield model; Het. = heterogeneous shield model.
[b]The poison pin diameter is reduced by a factor of 2.

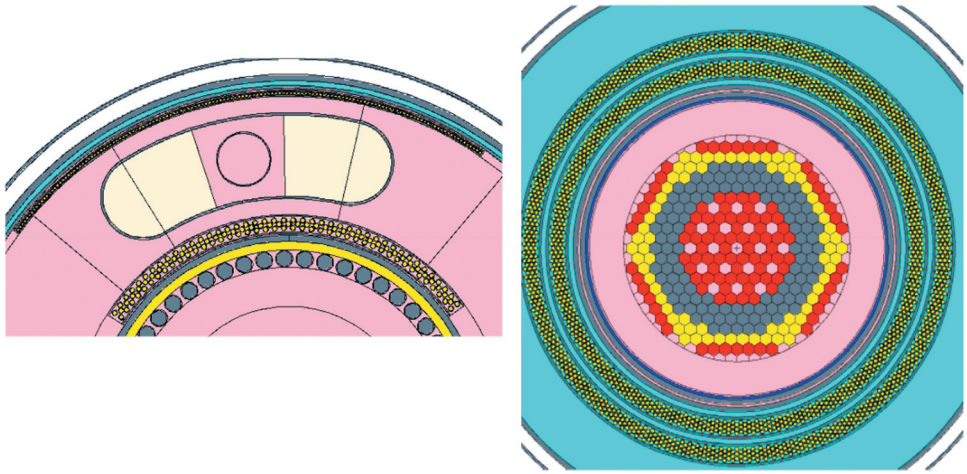

Fig. 4. The heterogeneous model of the (a) IHX and (b) core-level inner and outer shields.

between the homogeneous and the heterogeneous models has already been considered for the large safety margin currently used (a factor of 3).

The combined heterogeneity effect of the core-level inner and outer shields is slightly larger than that of the IHX shields. Unlike the heterogeneous IHX shield models, the heterogeneous core-level shield models result in a reduction of the secondary sodium activity by about 20%. While this is offset by the increase observed when using a heterogeneous model for the IHX shields, the secondary sodium overall activity is reduced by ~10% compared to the homogeneous models. Thus, it is recommended to use the homogeneous shield model for future scoping studies and to use the heterogeneous model once the shield designs are fixed.

TABLE IV

Comparison of Heterogeneous Core-Level Shield Model with Different Pin Diameters

Parameter	Original Case	New Case
Pin outer diameter (cm)	2.22	1.11
Number of rows	6	12
Flux (#/cm^2-s)[a]	2.28E+16	2.34E+16
^{10}B (n,α) one-group cross section (b)	2.28	2.26
Na activity ($\mu Ci/cm^3$)	2.06E-04	1.99E-04

[a]# = number of neutrons.

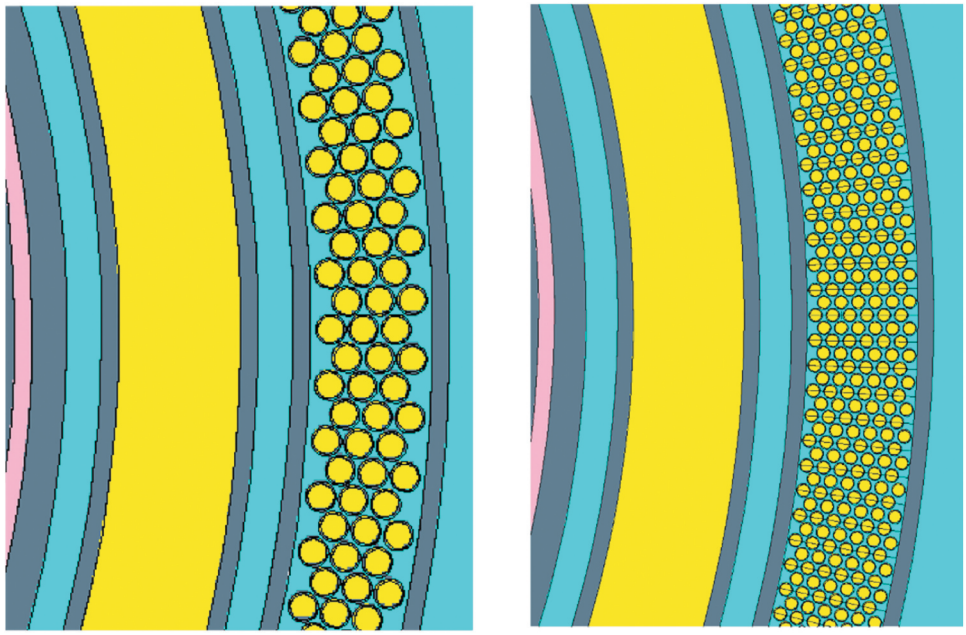

Fig. 5. Core-level shields with different pin diameters.

IV.E. Effect of Pin Diameter in Shield

The pin diameter effect of the core-level shields was investigated. Two cases using different pin diameters were compared and are summarized in Table IV. The MCNP models of the core-level outer shields for the two cases are presented in Fig. 5. The comparison shows that the effect of reducing the pin diameter has little effect on the secondary sodium activation rate in the IHX. The spatial and spectral self-shielding effects in these two cases are similar as observed from their similar ^{10}B (n,α) one-group microscopic cross section and flux levels in the B_4C rods. As part of this study, the cladding thickness was adjusted proportionally to maintain a constant steel volume fraction. The number of pins per row was also adjusted to maintain a constant B_4C volume fraction.

V. AIR ACTIVATION IN RVACS

The objective of the study is to assess the air activation inside the VTR RVACS. Outside air enters the RVACS chimney from the top and flows down to the bottom of the reactor vessel, where it is heated by the residual heat transferred from the core. The hot air rises to the top of the chimney and is returned back to the atmosphere. The natural flow is driven by the reactor decay heat. The purpose of the RVACS is to remove the reactor decay heat, but it is also continuously operating under a nominal condition but with a reduced flow velocity. The air gets irradiated and activated as it travels past the active core region. The small fraction of ^{40}Ar contained in the air is activated and becomes ^{41}Ar with a half-life of 109 min, which is released to the environment as air exits the RVACS. The radioactive isotopes produced and carried along with the air depend on the air composition and the pollutants or particles carried in the air. The air composition used in the study is listed in Table V. The concentration of pollutants or particles would depend on the actual reactor site, which is unknown at this stage and is not included in the activation analysis. However, the ^{41}Ar activity is expected to be the dominant contributor, so the analysis captures this major contributor.

TABLE V

Air Composition*

Isotope	Atom Percent
^{16}O	2.11E-01
^{17}O	8.02E-05
^{14}N	7.81E-01
^{15}N	2.89E-03
^{40}Ar	4.65E-03
Density (kg/m^3)	1.22

*Density used is at 20°C at atmospheric pressure.

TABLE VI

Input Parameters and Results for the Activity Assessment

Parameter	Value
Residence time in radiation zone (s)	15.9
^{41}Ar half-life (min)	109.34
^{41}Ar production rate (#/s)[a]	5.19×10^{8}
^{41}Ar activity at the exit (μCi/cm^3)	6.39×10^{-8}

[a]# = number of productions.

Similar to the secondary sodium calculations, Eq. (2) was solved to calculate the ^{41}Ar activity at the exit of the RVACS. The only difference is that the exiting air is assumed to not be recirculated into the system. The value S now is the production rate of ^{41}Ar, i.e., the ^{40}Ar capture reaction rate, and is a function of the position along the flow path. It was assumed that activation occurs only from the bottom to the top of the vessel. Activation in other areas (e.g., in the chimney) is deemed negligible due to their being far away from the neutron source that is the reactor core.

Applying the boundary condition ($t = 0$ corresponds to the entrance into the radiation zone) and solving the equation assuming that the production rate is constant over the domain, the result is

$$N(t) = \left(\frac{S}{\lambda}\right)\left(1 - e^{-\lambda t}\right),$$

where t is the time spent by air in the activation zone (near the core). It is usually much smaller than the ^{41}Ar half-life, and therefore, at the exit of the radiation zone, we have

$$N \approx St.$$

It is recognized that the production rate will vary at different positions along the air flow path. In addition,

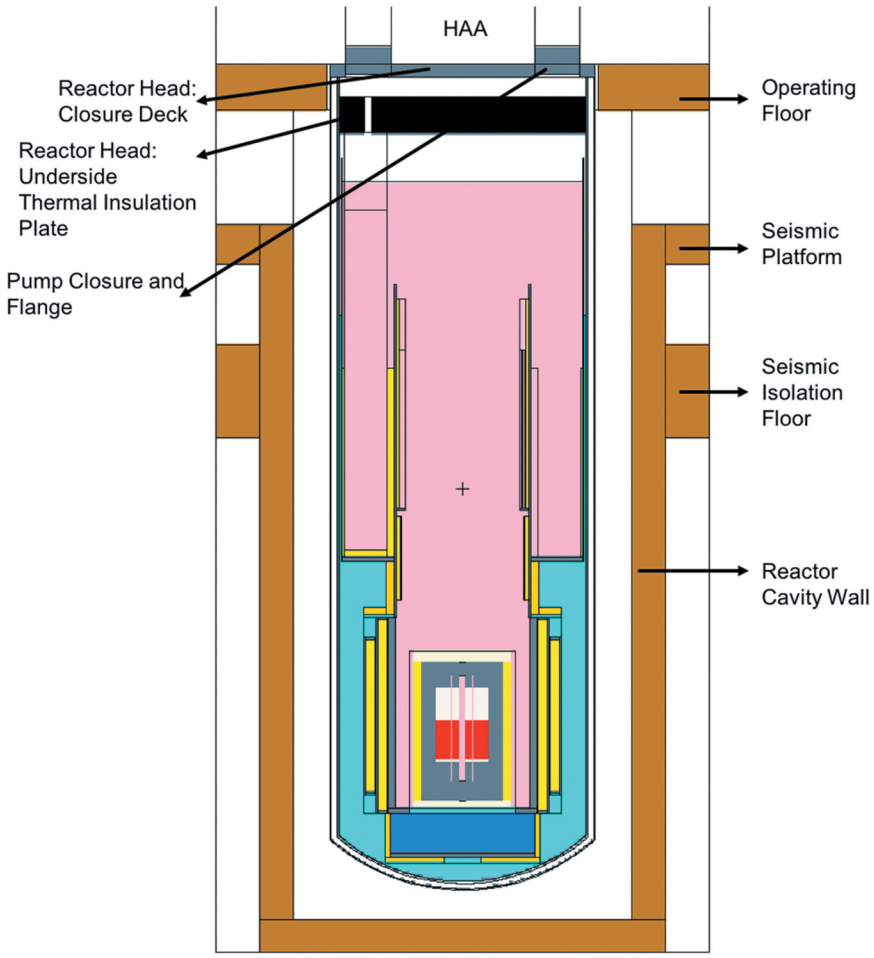

Fig. 6. Expanded MCNP model for dose rate evaluation above the operating floor and HAA.

the air density will be slightly changing with temperature and pressure. Neither of these refinements is considered in the current model at this stage.

The input parameters used for the calculation and the results are listed in Table VI. The activity is calculated at the exit of the RVACS chimney.

VI. HAA DOSE RATE

TABLE VII

The Primary Sodium Activation Rate in VTR

Region	Sodium Volume (cm^3)	Reaction Rate (#/s)[a]		
		Capture	(*n*,*p*)	(*n*,2*n*)
Cold Na	7.68E+07	1.39E+13	—[c]	—[c]
Core[b]	6.76E+06	1.56E+17	6.68E+15	3.49E+13
Hot Na	1.48E+08	1.01E+16	5.41E+13	—[c]

[a]# = number of reactions.
[b]The Na volume fraction in the core is about 41% including the gap sodium inside the barrel.
[c]MCNP tallies have large statistical errors (>10%), and the mean value is several orders of magnitude smaller than the capture rate.

TABLE VIII

Primary Sodium Activity of the VTR Core

Parameter	Value
^{24}Na activity (μCi/g)	23 046
^{22}Na Activity (μCi/g)	4.88

The objective is to evaluate the dose rate above the HAA and the operating floor adjacent to the HAA. The MCNP6.2 model developed for the IHX secondary sodium activation analysis and the RVACS air activation analysis was expanded to include additional features important to this problem as illustrated in Fig. 6. Preliminary simple analyses have shown that the fission neutrons correspond to only a small fraction of the dose rate above the HAA. The focus of this study was mainly on the activated primary sodium, which is the major source contributing to the dose rate above the operating floor and the HAA during operation. The calculation procedure has two steps. The first step evaluates the primary sodium activation. The upper internal structure (UIS) was not modeled. This would overestimate the primary sodium activation rate in the hot sodium pool. However, the overestimation is small since the primary sodium is mainly activated when flowing through the active core region. The second step used the calculated photon source for a fixed source calculation to evaluate the dose rate above the operating floor.

The ^{23}Na capture, (*n*,*p*) and (*n*,2*n*) reaction rates were evaluated by MCNP6.2 for the hot pool, the cold pool, and the core region. The results are listed in Table VII. It is observed that the capture rate is several orders of magnitude larger than the (*n*,*p*) and (*n*,2*n*) reactions; i.e., the ^{24}Na decay is the major contributor to photon emission during normal reactor operation. This source is assumed to be uniformly distributed in the core, the hot pool, and the cold pool. The specific activity of ^{24}Na was calculated based on the total reaction rate and the sodium volume given in Table VII. The results are listed in Table VIII.

Based on the photon source obtained from the first step calculation, the photon transport calculation was conducted with MCNP6.2. Several cases were assessed, with results listed in Table IX. The dose rates above the HAA and the operating floor were investigated separately as different weight windows were needed for all the different cases. It was observed that the streaming paths through the pump and IHX openings are important above the HAA as illustrated in Fig. 7. Pump closures and flanges serve the purpose of blocking the streaming path through the pump as shown in Table IX. The dose rate near the IHX penetration is also around 1000 mrem/h. An additional 10 to 20 cm of steel shield may be needed around the IHX penetrations to block these streaming paths depending on the radiation zone classification. The calculations will be revisited as the overall plant design matures.

By comparing Cases 3 and 4, we observed that the density of the concrete is not an important factor since the major photon streaming path is through the 3-in.-thick gap between the HAA deck and the operating floor as illustrated in Fig. 8. The 3-in.-thick gap is there to accommodate potential thermal expansion of the vessel. The maximum dose rate that took place directly above the gap is around 80 000 mrem/h. Shielding is intended to be placed around the gap to prevent the particle streaming through the gap, but geometrical details are still being worked out. By filling in the gap (Cases 5 and 6) with a made-up model, the dose rate on the operation floor is significantly reduced. The density of the operating floor has a significant impact on the dose rate.

TABLE IX

Dose Rate Above the HAA and the Operating Floor

Case	Location	Description	Dose Rate (mrem/h)
1	HAA	Without pump closure and flange	1412.90
2	HAA	With pump closure and flange	0.02
3	Operating floor	Regular concrete (density = 2.3 g/cm^3)	56.21
4	Operating floor	High-density concrete (density = 4.0 g/cm^3)	54.41
5	Operating floor	Gap filled with 1-m-thick Type 314 stainless steel	0.11
6	Operating floor	Gap filled with 0.5-m-thick Type 314 stainless steel	0.28
7	Operating floor	Shielded streaming path and high-density concrete	3.84×10^{-3}
8	Operating floor	Shielded streaming path and regular concrete	0.94

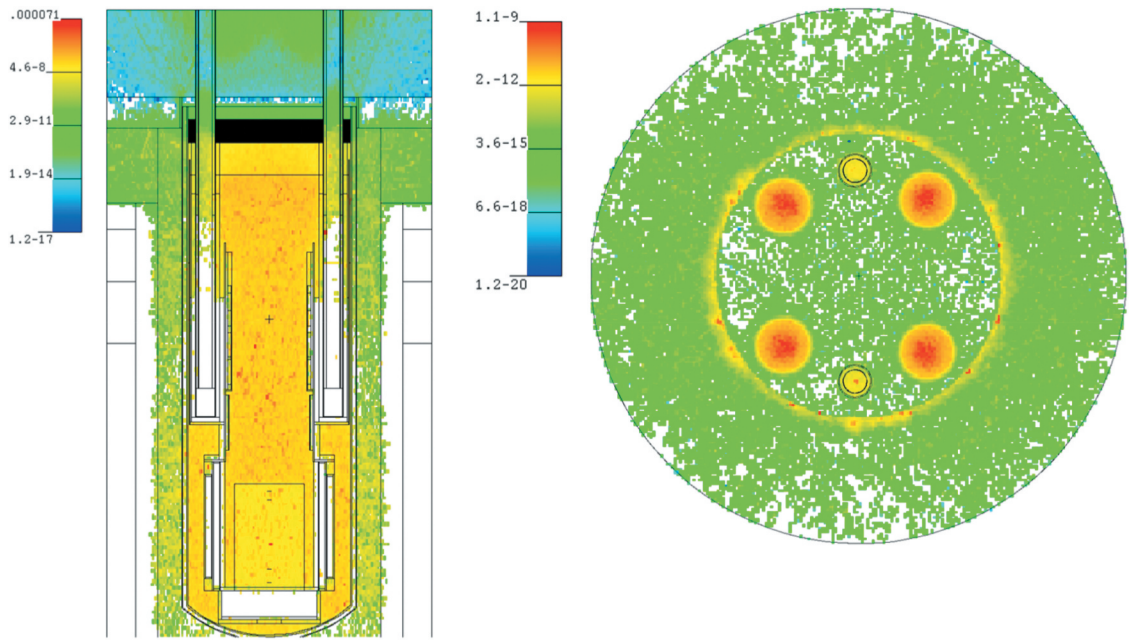

Fig. 7. (a) Axial photon flux distribution and (b) radial photon flux distribution above the HAA.

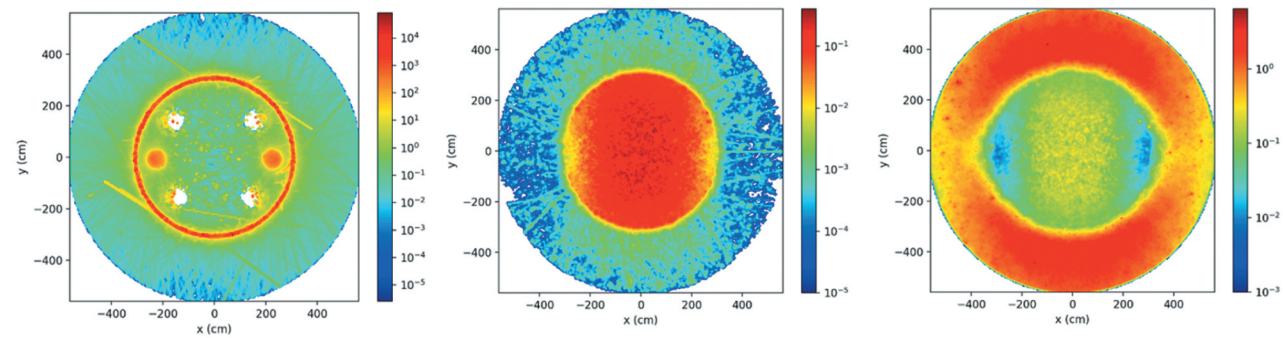

Fig. 8. The radial photon dose rate distribution above the reactor head for (a) Case 4, (b) Case 7, and (c) Case 8. Note that the color scale is different in each figure.

However, if the radiation zone classification for this region sets the limit at 2.5 mrem/h, then regular concrete will be sufficient to satisfy this limit.

VII. CONCLUSION

Shielding analyses were performed for the reference conceptual VTR design. The main areas assessed include the secondary sodium activation in the IHX, the air activation in the RVACS, and the dose rate evaluation above the HAA and the operating floor. The main streaming paths to these regions of importance were identified, and the activation and dose rates were evaluated based on the current shielding configuration and reactor design information. The effectiveness of the shield components to minimize and mitigate these streaming paths was also evaluated. As the VTR design progresses and more detailed design information becomes available, the shielding analyses and the calculation models discussed in the study are expected to evolve accordingly. The purpose of these analyses is also to provide information to inform the plant and core design activities and ensure that shielding and radiation protection aspects are properly accounted for.

Acknowledgments

This paper was created by UChicago Argonne, LLC, Operator of Argonne National Laboratory, which is a DOE Office of Science laboratory operated under contract number DE-AC02-06CH11357. The work reported in this paper is the result of ongoing efforts supporting the VTR.

Disclosure Statement

No potential conflict of interest was reported by the author(s).

References

1. F. HEIDET and T. FEI, "Updated Reference VTR Core for CD-1," ECAR-4647, Argonne National Laboratory (2019).
2. S. E. BAYS and T. FEI, "Calculation of Neutron Damage to Sodium Coolant Inlet Plenum," *Trans. Am. Nucl. Soc.*, **121**, 1403 (Nov. 2019); https://doi.org/10.13182/T31005.
3. B. S. TRIPLETT, E. P. LOEWEN, and B. J. DOOIES, "PRISM: A Competitive Small Modular Sodium-Cooled Reactor," *Nucl. Technol.*, **178**, *2*, 186 (2012); https://doi.org/10.13182/NT178-186.
4. C. J. WERNER, "MCNP Users Manual – Code Version 6.2," LA-UR-17-29981, Los Alamos National Laboratory (2017).
5. S. W. MOSHER et al., "ADVANTG—An Automated Variance Reduction Parameter Generator," ORNL/TM-2013/416, Rev. 1, Oak Ridge National Laboratory (2015).
6. A. KASAM-GRIFFITH et al., "VTR Core Design for Flexible Operations" (submitted for publication).
7. T. E. BOOTH and J. S. HENDRICKS, "Importance Estimation in Forward Monte Carlo Calculations," *Nucl. Technol./Fusion*, **5**, *1*, 90 (Jan. 1984); https://doi.org/10.13182/FST84-A23082.
8. INTERNATIONAL COMMISSION ON RADIATION AND PROTECTION, "Data for Protection Against Ionizing Radiation from External Sources: Supplement to ICRP Publication 15," ICRP Publication 21, Pergamon Press, Oxford (1973).
9. T. FEI et al., "SINBAD Shielding Benchmark with MCNP6 and MC2-3/TWODANT," *Trans. Am. Nucl. Soc.*, **119**, 1026 (2018).